European Master in Theoretical Chemistry and Computational Modelling

MASTER THESIS

DIELECTRIC CONSTANT IN ENDOFULLERENES

June 16, 2017

Alejandro Díaz Márquez

Supervisors: Selim Sami, and Dr. Remco W. A. Havenith

University of Groningen
Zernike institute for advanced materials
alejandro_92_6@hotmail.com

Contents

1 Introduction

Global warming is one biggest concerns of this century, which is partially generated by the combustion of fossil fuels. In order to fight against the climate change problem, and keep supplying the global energy demand, the non-renewable resources must be replaced by other resources, which can reduce or banish the negative impact on the environment. Renewable energies are based on natural resources [1], which are naturally replenished on the human time-scale.

It is widely known that one renewal resource is the solar energy in which sunlight is transformed into electrical current by the photovoltaics cells. These devices are semiconductor materials, which have a suitable band gap (crystal structures), or HOMO-LUMO gap such as molecular materials. In the following figure, different kinds of photovoltaics cells are represented, comparing their power efficiencies over the years:

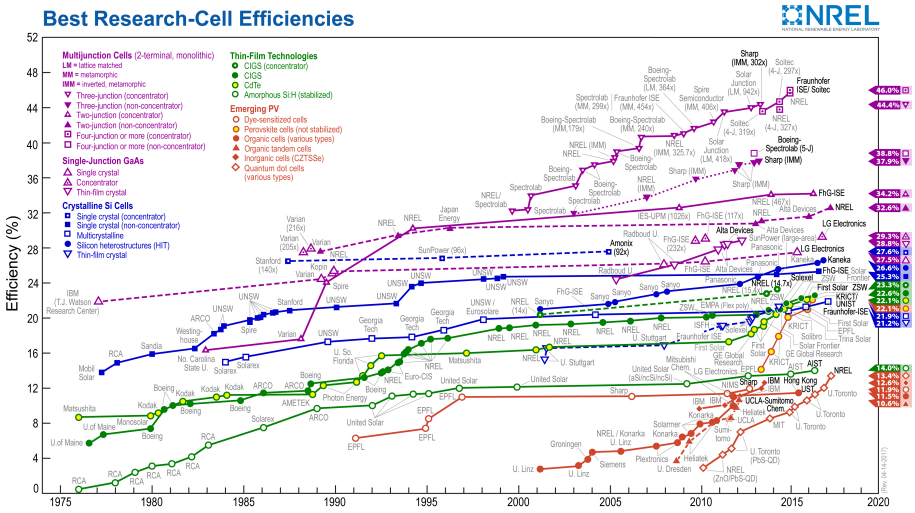

Figure 1: Power efficiency as a function over the years for different types of solar cells [2]

The first photovoltaics cells were based on inorganic semiconductors like Si, GaAS or CdTe crystalline compounds with power efficiencies relatively low. During this century, photovoltaic cells have evolved in order to new devices with higher power efficiencies, the highest are around 46% of energy conversion, hence their production cost is high. Furthermore, new photovoltaic materials are emerging in parallel. One promising field is the organic photovoltaics (OPVs), because of low production cost, and their flexibility compared with the other semiconductors devices. The main disadvantages is the relatively low power efficiency, around 12%, about 3 times lower than the inorganic devices.

1.1 Organic photovoltaics

This category of solar cells is based on organic electronics, which deals with semiconductive organic polymers or small organic molecules [3]. The reason for using polymers is that the molecules must be highly conjugated, in order to reduce the ($\pi \rightarrow \pi^*$) transition gap, until reaching the optimal band gap for the sunlight absorption process. In this particular system, the delocalized π orbital, which is the highest occupied molecular orbital (HOMO), takes the role of the valence band, while the π^* orbital, which is the lowest unoccupied molecular orbital (LUMO), corresponds to the conduction band.

The main issue of organic photovoltaics is the exciton dissociation [4], which is a bound state of an electron and an electron hole which are attracted to each other by the electrostatic Coulomb force, see figure 2. Therefore, the electron remains near the molecule unlike the electrons in the inorganic semiconductors, where they can freely move once they are excited to the conduction band.

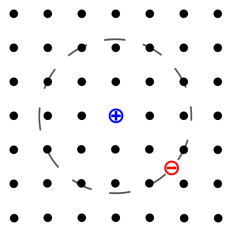

Figure 2: Frenkel exciton representation, where the hole (blue plus) is in the centre of the crystal (black dots), and the electron (red minus) feels the attraction of the hole. Figure from *wikimedia commons*[5].

The most commonly used approach to reduce the problem of bound excitons is to use donor (D) and acceptor (A) materials, represented in figure 3 and combine them in a bulk heterojunction. These acceptors materials have a high affinity, such as fullerene derivatives, which can take the excited electron and reduce the dissociation barrier of the exciton binding state:

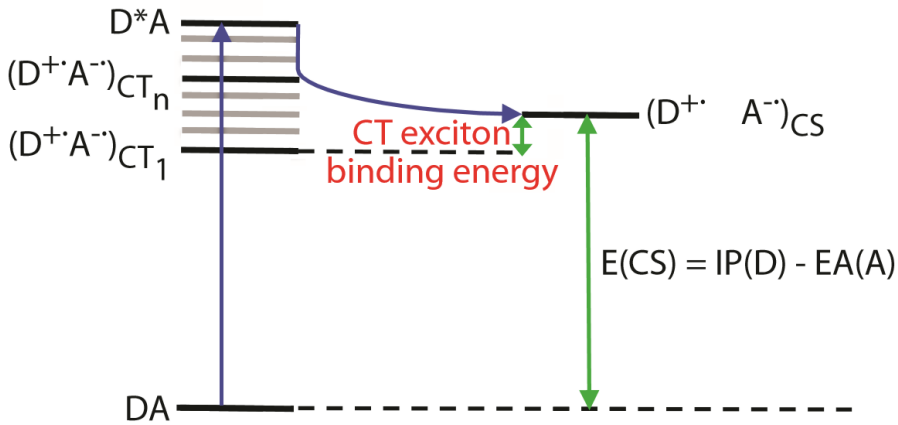

Figure 3: Electronic state diagram of the working mechanism of an organic solar cell. Figure from Hilde D. de Gier [6]

As we have introduced previously, the donor part (D) constitutes of conjugate polymers, where usually the excitation process takes place, ($DA \rightarrow D^*A$). The generated exciton must diffuse to the donor/acceptor interface, where the charge is transferred ($D^*A \rightarrow (D^{+\cdot}A^{-\cdot})_{CT}$) to the acceptor ($A$), before the electron return to the donor (D) due to recombination process.

During the charge separation process, the exciton bound state must be broken into free radicals ($(D^{+\cdot}A^{-\cdot})_{CT} \rightarrow (D^{+\cdot} + A^{-\cdot})_{CS}$). It is proposed that the low dielectric constant of organic photovoltaics will helps to the exciton be still present even at larger distances. Actually, one new challenge is thus the design of new organic materials for solar cells with high dielectric constants. Some of these materials are the PTEG-1 or PTEG-2, which are fullerene derivatives with chains of triethylene glycol, with a dielectric constant of 5.7 and 5.2 respectively [7], which is still low compared with the silicon 11.7 [8].

Recently, experimentalists have successfully inserted water and other small molecules in fullerene cages [9, 10]. Small molecules with a high dipole moment, and probably combined with the free movement may increase the dielectric constant of the whole system. These endofullerenes are an interesting option for increasing the dielectric constant without altering the morphology of the system.

2 Objective

The dielectric constant is a macroscopic property, which can be determined by classical molecular dynamics. However, the particularity of endohedral fullerenes, where the inner particle remains isolated from the external medium, generates a new environment, which cannot be described by the available forcefields. Therefore, the main focus of this project is the quantum mechanical study of the water molecule inside the C_{60} to determine the electrostatic interactions between water and C_{60} and be able to parametrize a specific forcefield for this system, calculating energy diagrams for water mobility, dipole moments for electostatic interaction, and density for charge transfer processes. Once the system is properly described, and a new forcefield is parametrized, the dielectric properties can be obtained. Moreover, other molecules has been studied inside the C_{60}, like hydrogen fluorine and hydrogen iodine, and compared with the water system.

3 Theoretical background

In this chapter, I will introduce some theoretical concepts behind the calculations performed in order to describe water in C_{60}.

3.1 Dielectric constant

The dielectric constant is a macroscopic property, which modifies the Coulomb force between two point charges in a material, depending on the frequency of the applied field. It is also known as the relative permittivity (ϵ_r), that is the ratio between the permittivity of a certain medium (ϵ) relative to that of the vacuum permittivity (ϵ_0).

$$\epsilon_r = \frac{\epsilon}{\epsilon_0} \tag{1}$$

Moving this definition into photovoltaic field, the dielectric constant could be related to the charge separation efficiency [11], represented in figure 3. Therefore, materials with a high dielectric constant could increase the power efficiency due to the reduction of the exciton binding energy. In the next figure 4, the three contributions of the dielectric constant are represented in function of the frequency of the applied field.

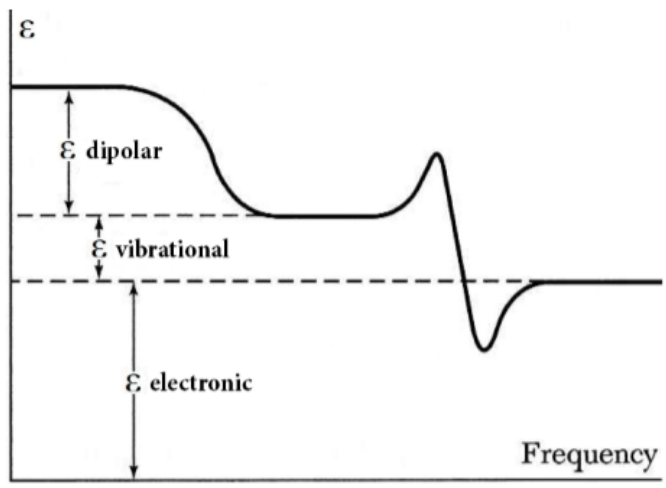

Figure 4: This figure represents the dielectric constant as a function of the frequency of an electric field, and the three contributions (dipolar, vibrational, and electronic) of the total dielectric constant. Figure adapted by Selim Sami, source from [12]

These three contributions are represented in the above figure 4.

1. The first one is the dipolar contribution, which is relevant for molecules with permanent dipole moments. When an electric field is applied, the molecule reorients by rotational and translational movements. Since these reorientations occur at relatively long time scales, the dielectric constant of this contribution is only visible at lowest frequencies.

2. The second one is the vibrational contribution, which is due to small movements along the vibrational normal modes of the molecule in the presence of an external electric field.

3. The last one is the electronic contribution, which represents the electronic behaviour of the molecule, describing the polarizability of the material.

The first two contributions can be easily studied form a classical point of view, because they are properly described by forcefields. However, studying the third contribution classically is more complex, for this case a molecular polarization should be included, but we will discus this problem with more details in the following section. In any case the electronic contribution can be properly studied from a quantum mechanical calculation.

In order to get the dielectric constant from a classical point of view, the dipole fluctuation method has been applied. This method calculates the vibrational and dipolar dielectric constant ($\epsilon^{vib+dip}$) from the fluctuations of the total dipole moment ($\langle\mu^2\rangle - \langle\mu\rangle^2$) of the system throughout the simulation. Here, (V) is the volume, (k_b) is the Boltzmann factor, and (T) is the temperature:

$$\epsilon^{vib+dip} = \frac{4\pi}{3}\frac{\langle\mu^2\rangle - \langle\mu\rangle^2}{Vk_bT} \tag{2}$$

On the other hand, the electronic part of the dielectric constant can be obtained from the polarizability of the material by using the following bulk equation, which is derived from the Lorentz field [13], where (χ_e) is the electric susceptibility, (V) the volume, and (α) the polarizability:

$$\epsilon^{elec} = 1 + \chi = 1 + \frac{4\pi}{V}\alpha \tag{3}$$

Now the unknown variable is the polarizability of the material, which can be obtained from the second derivative term of the energy by using the coupled perturbed method Kohn-Sham (CPKS), where the applied electric field is dealt as a perturbation:

$$E_{tot} = E^0_{tot} - \sum_{\beta}\mu_\beta\varepsilon^0_\beta - \frac{1}{2}\sum_{\beta,\gamma}\alpha_{\beta\gamma}\varepsilon^0_\beta\varepsilon^0_\gamma... \tag{4}$$

Here, the dipole moment (μ_β) is obtained from the first derivative, and the polarizability ($\alpha_{\beta\gamma}$) from the second derivative.

3.2 Polarizable forcefield

In the case of classical dynamics, the electrostatic interactions are represented by point charges that are kept constant during the simulation. This approximation completely neglects the electronic polarizability, which can be important in specific systems.

The polarizability can be artificially added to the forcefield in multiple ways. In our simulations, we used a polarizable forcefield based on the Drude particle [14]. This particle represents the electron cloud with a negative point charge and the atom represents the protons with a positive point charge. These particles are then connected with an harmonic spring and the point charge (q_D) can be obtained by the following equation, where (k_D) is the force constant and (α) is the polarizability.

$$\alpha = \frac{q_D^2}{k_D} \tag{5}$$

In figure 5 below, a water molecule with a Drude particle can been seen.

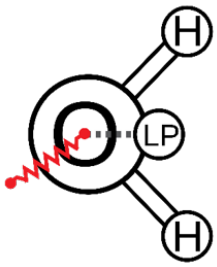

Figure 5: This figure represents 4-sites water model, where the Drude particle (red line) is attached to the oxygen by an harmonic constrain

4 Computational details

During this section, I will explain all the computational details, and programs employed in order to carry out all the calculations, and simulations.

4.1 Quantum mechanics

Geometries of fullerene-C_{60} containing water, HF or HI inside were optimised in the gas phase using DFT (6-311G**/B3LYP) with the program Gamess-UK [15]. Spherical harmonics are used in order to avoid linear dependencies. The electronic integration was performed numerically with a very high quadrature grid, and the precision has been increased until the sixth decimal (E-6) in order to avoid imperfections of the SCF convergence during the optimisation. Choosing a small quadrature grid may generate non converged energies in this system. Finally, the Grimme-D2 dispersion correction [16], proposed by Stefan Grimme for density functional calculations, has been used in order to improve the description of the long range correlation effects.

Moreover, atomic charges were obtained using two methodologies: Mulliken analysis, and dipole preserving analysis (DPA) [17]. Finally, the charge transfer process has been studied by means of differences in the density of $H_2O@C_{60}$ system minus the densities of water, and C_{60}, each calculated separately. In order to obtain the density, 3D grid densities were generated using a cubic box of 20 Bohr in length, centred around the C_{60} molecule, with a sampling of 750 points for each axis. In all cases, the analysis were performed at the same precision level as geometry optimisation.

Furthermore, periodic DFT (6-31G(d,p)/PBE) calculations were performed with the program CRYSTAL [18] in order to obtain the electronic dielectric constant in the solid. These calculations were performed by Selim Sami.

4.2 Molecular dynamics

Thermodynamic and dielectric properties of water in C_{60} were simulated in a crystal structure using standard and polarizable forcefields available in the literature with the program GROMACS 5.1.2 [19]. The C60 fullerene topology has been taken from Monticelli [20], where the C_{60} geometry came from NMR data [21], bond lengths and angle from OPLS-AA forcefield [22], and Lennard-Jones parameters from Girifalco [23]. Moreover, the SPC water model [24] has been used for standard forcefield simulations, while the SWM4-NDP 4-site polarizable water model [25] was used for polarizable forcefield simulations. The spring constant for the C_{60} atoms was the same as water model ($k_D = 418400 kJmol^{-1}nm^{-2}$), a partial mass of 0.4 atomic unics has been subtracted from carbon atom in order to provide a Drude particle mass, and arbitrarily 0.5 positive charge was applied for carbons, and 0.5 negative charge for the Drude particle.

All the simulations were performed under the isothermic-isobaric ensemble (NPT) with a temperature of $298.15K$, and a pressure coupling of $1bar$. Simulation conditions were taken from Monticelli [20]: Noose-Hoover thermostat with $\tau_t = 1.0ps$, Parinello-Rahman barostat with $\tau_p = 4.0ps$ and compressibility of $0.00045bar^{-1}$, PME electrostatic interaction, integration step of $0.002ps$, and $1.1nm$ cut-off for Lennard-Jones and Coulombic, although this cut-off was reduced for small boxes. In the case of polarizable forcefield simulations, the time step was reduced until $0.0006ps$, the thermostat was V-rescale, and the barostat was Berendsen.

5 Results and discussion

Previously, quantum mechanical calculations in periodic systems were carried out to obtain the electronic dielectric constant. These results did not show any significant increment of the dielectric constant, when a water molecule is inserted in the C_{60}, which is reasonable because of the relative low electronic density of water compared with the C_{60}. Therefore, the variations in the dielectric constant will be affected by the dipolar, and vibrational contributions. These contributions can be calculated as fluctuations of the dipole moment over time using molecular dynamics simulations. However, this system has not yet a proper forcefield, which can describe these interactions. In the following section, we carried out a quantum detailed description of this system in order to get enough information to parametrize a forcefield.

5.1 Water molecule in C_{60}

The first step was the optimization of the water molecule in the C_{60}, which is represented in the two following figures 6.

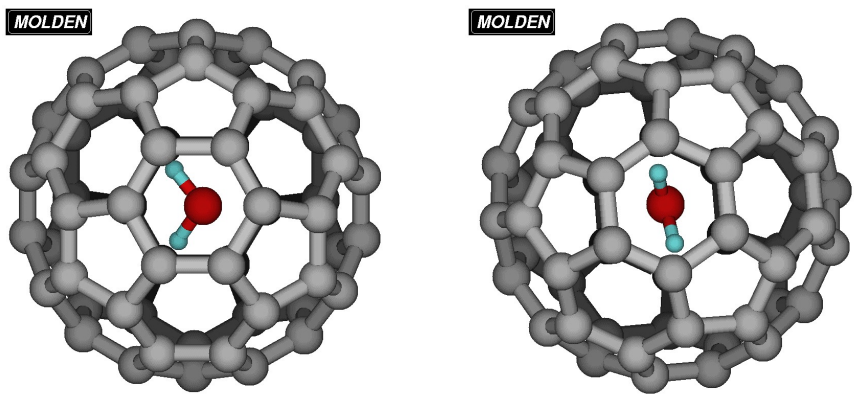

Figure 6: Optimized geometry of $H_2O@C_{60}$ from a lateral (left image), and frontal (righ image) points of view, images generated with molden software [26]

We can deduce from these images that water molecule has a preference for the centre rather than being attached to the C_{60} surface, and also oriented to the hexagonal faces. This result is quite coherent, since the C_{60} are spherical molecules, their lowest electronic density is located at the centre, and because of that the water molecule feels the lowest repulsion in this region. The next step was an energy barrier calculation, where we carried out constrained optimizations at different points in space, displacing the water molecule through the centre:

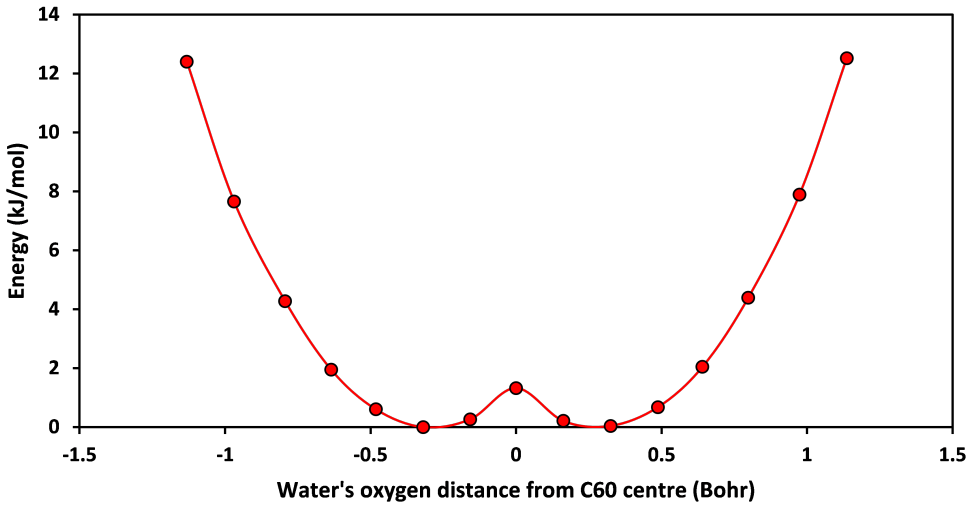

Figure 7: Energy representation of the water's oxygen molecule as function of the distance from the C_{60} centre

In figure 7, we can observe that water's oxygen is slightly biased from the centre, around 0.32 Bohr, which generates two minimas. In both cases the oxygen of the water molecule moves towards the C_{60}, leaving the centre of mass of water near the C_{60} centre. Although, there is a small energy barrier ($\approx 2kJ/mol$) between the two minimas, the water's oxygen can easily reach this position, because this energy barrier is lower than the kinetic energy available at the room temperature (298.15K) ($\bar{E}_{298.15} = \frac{3}{2}k_BT \approx 3.72kJ/mol$), allowing also translation movements in this region. Moreover the rotation has been studied using single points calculations, where the water molecule was rotated around the centre of C_{60} in the xy-plane:

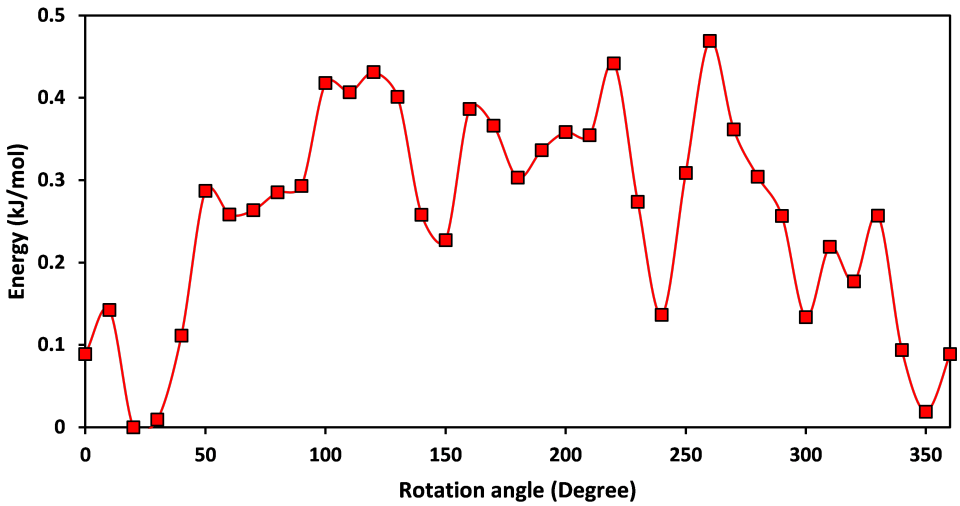

Figure 8: Energy representation of the water's oxygen molecule as function of the xy-rotation angle

As we can see in the figure 8, the required energy to rotate the water molecule is even lower than the translational barrier, thus allows a completely free rotation of water, which is extremely beneficial for high dipole fluctuations. Furthermore, we moved the water's oxygen to further distances in the C_{60} in order to study how the energy increases when the water is closer to the fullerene:

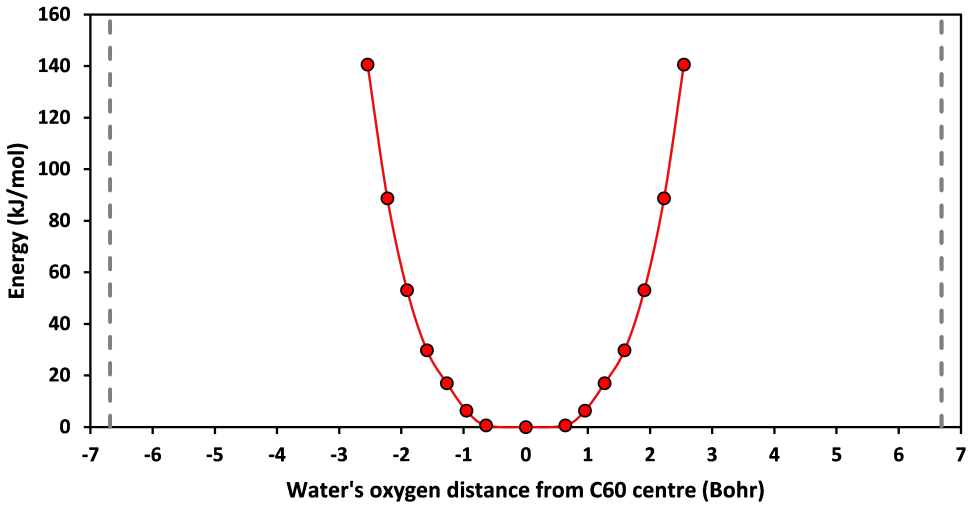

Figure 9: Energy representation of the water's oxygen molecule as function of the distance from the C_{60} centre (red lines), the position of the C_{60}'s carbons are represented by grey dotted lines.

In figure 9, we observe a high increment of the energy, when the water distances from the C_{60} centre. We can roughly consider that the water molecule cannot go further than two Bohr approximately, which represents an energy barrier around 60 kJ/mol. We can conclude that the water molecule is well localized in the centre of the C_{60}, but with enough translational and rotational freedom.

In the following step, we studied the behaviour of the water molecule in more details, where we carried out the same calculations of the figure 7, but in this case we fixed the orientation of the water molecule in order to observe how the hydrogens interact with the C_{60}:

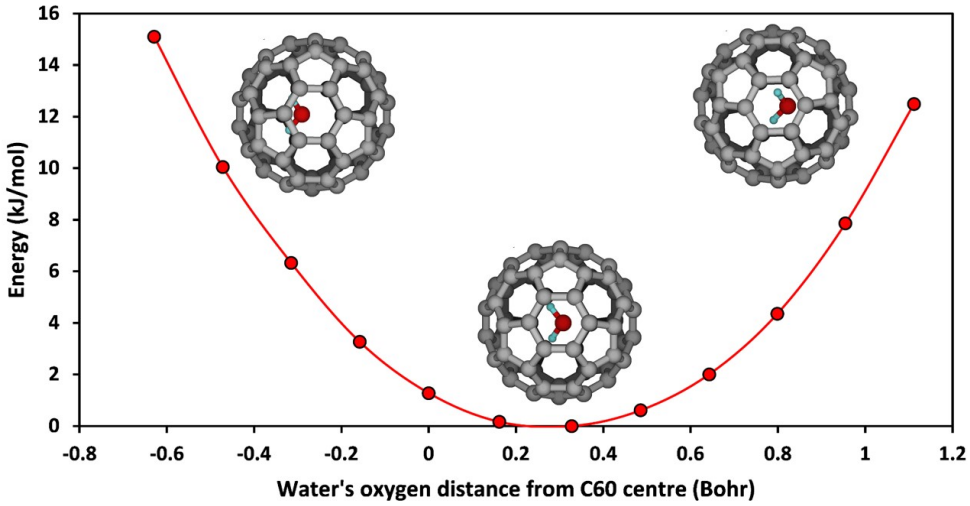

Figure 10: Energy representation of the water's oxygen molecule as a function of the distance from the C_{60} centre (red lines), $H_2O@C_{60}$ molecules are included showing the relative position of the water in the C_{60}.

Comparing this figure 10 with figure 7, the hydrogens interaction with the C_{60} is relatively higher in energy than oxygen interacting with the C_{60}, which means some attractive interaction, like polarization, between water's oxygen and C_{60}. Moreover, we calculated the bond lengths and angles as function of the distance from C_{60}, where the water bond distances are (1.815±0.004 Bohr), unaffected by the position. However, the water angle is slightly distorted when the hydrogens goes closer to the C_{60}. Even if this variation is relatively small, around 1 degree, it could have a significant effect on the water dipole moment. Therefore, the dipole moment, and the atomic charges has been calculated using the Mulliken and DPA analysis.

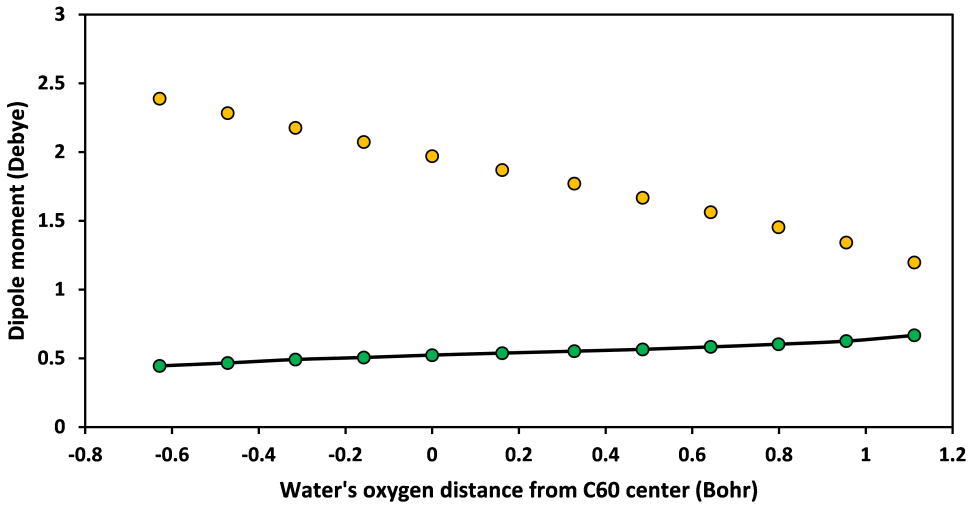

Figure 11: Dipole moment calculation using Mulliken analysis (yellow dots), and dpa (green dots), compared with the dipole moment calculated with wavefunction (black line)

As we see in figure 11, it is confirmed that DPA perfectly describes the dipole moment over the whole space, but it is not the same thing for Mulliken analysis, which always overestimates the dipole moment, hence DPA the analyis gives a better description for this system. Moreover, the DPA dipole moment is significantly lower than free water dipole moment, which is 2.06 Debye, and also it slightly increases when the oxygen approaches the C_{60}. These two results show a response of the C_{60} due to the water, which represents the polarization. Therefore, we calculated the charges of the whole system in order to understand the low dipole moment. In the following plot only water charges are represented:

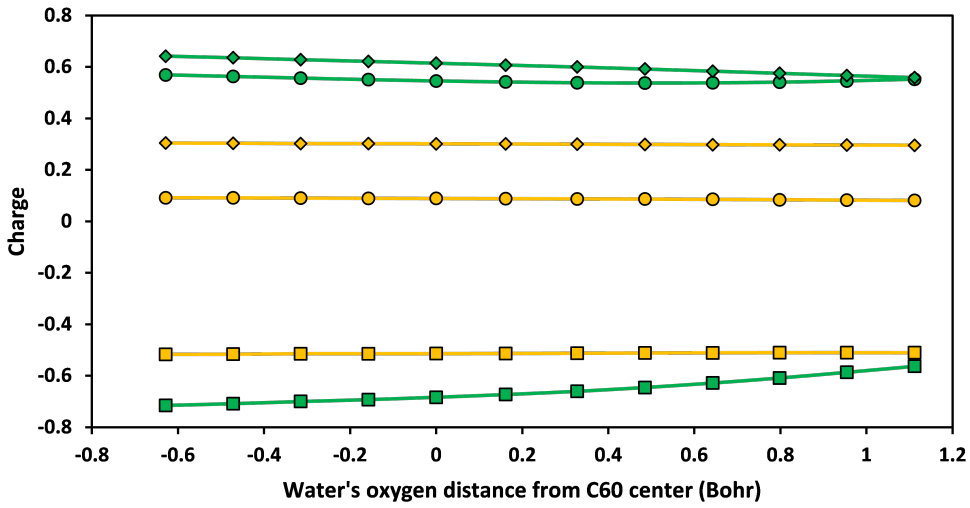

Figure 12: Representation of mulliken charges (yellow), and dpa charges (green): oxygen charge is represented by squares, hydrogens by diamonds, and the total charge by spheres.

We observe that the DPA charges shown in figure 12 are larger than the the Mulliken charges, but as we have seen before, the DPA dipole moment is lower than Mulliken dipole moment. The key point is that the total water DPA charge is not neutral, it is around 0.55, while for Mulliken charges it is around 0.088. Consequently, the missing charge thus electrons shift from water to C_{60}, which is distributed in the way to counter the DPA charge, hence the C_{60} is polarized. However, since this charge is relatively high, this could mean also charge transfer from the water molecule to the C_{60}.

5.2 Density

In order to determine if charge transfer takes place, three density grids $H_2O@C_{60}$, water and C_{60} where generated using the same box size and number of grid points as we described in computational details section, thus obtaining the same precision level for the density subtraction. In the $H_2O@C_{60}$ density grid, we performed a radial integration starting from the centre of the C_{60} molecule until reach 10 Bohr, which is the limit of the box, see figure 13:

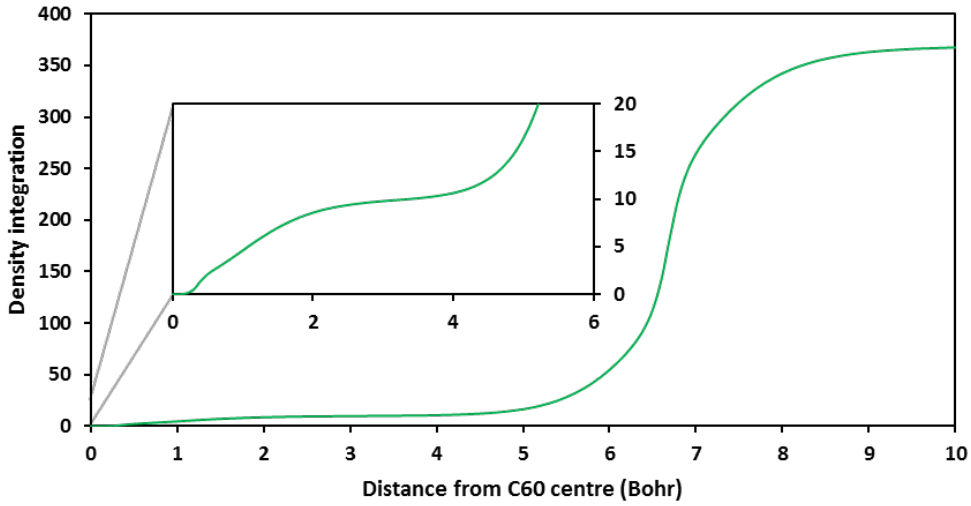

Figure 13: Density radial integration from the C_{60} centre until the limit of the box

The total radial density integration from 0 to 10 Bohr gives a number of 368.39 electrons, that means an error lower than 1% from the exact value of 370 electron, which is relatively small around 1.65 electrons. Considering that our objective is to calculate the charge transfer, which is a small perturbation in the density, this error is quite large and can cause wrong results. If we examine in more detail, an inflection appears in the region between 2 and 4 Bohr over the density integration. This inflection point means that the density integration does not increase between this region, that means a minimal in the density, as we can see in the following figure:

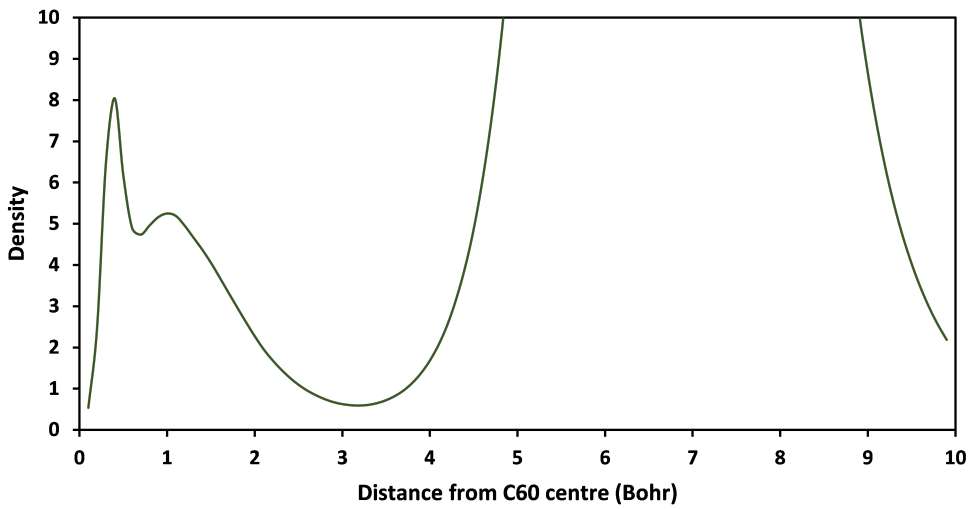

Figure 14: Radial density of $H_2O@C_{60}$ from the C_{60} centre until the limit of the box

Figure 14 shows the radial density of the water molecule, where the first peak around 0.4 Bohr corresponds to the oxygen electronic density. From approximately 0.7 to 3 Bohr approximately, the electronic density of the hydrogens is represented. Finally, the electronic density of the C_{60} starts around 4 Bohr. Therefore, we can deduce that there is a region where the density is minimal

inside the C_{60}. To study this region, we generated a 2D plot, where we represented all the minimal grid points in a $H_2O@C_{60}$ slice that is 0.52 Bohr thick.

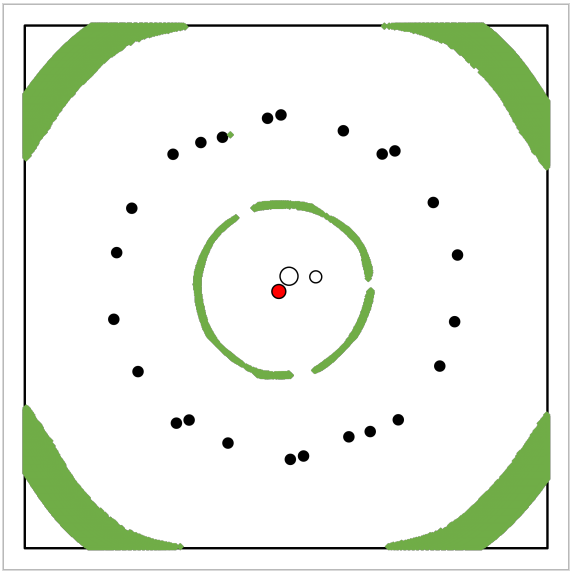

Figure 15: 2D $H_2O@C_{60}$ representation with: oxygen red dot, hydrogen white dots, C_{60}'s carbons black dots, green points are the minimal values of the density

As observed in figure 15, the density minimals points represented in the inner region of the C_{60} have an spherical shape, which validates the radial integration of figure 13. Moreover, the radius of the inflection point is located at 3.2 Bohr from the centre, this value has been calculated using the symmetric different quotient derivative operation [28].

$$f'(x) = \frac{f(x+h) - f(x-h)}{2h} \tag{6}$$

Finally, the charge transfer was calculated as the density difference between the $H_2O@C_{60}$ complex and water and C_{60} separately ($\delta\rho = \rho_{water@C60} - \rho_{water} - \rho_{C60}$). Using this strategy, the missing electrons due to the grid precision is reduced, since all the densities are represented by the same number of points, the errors cancel out.

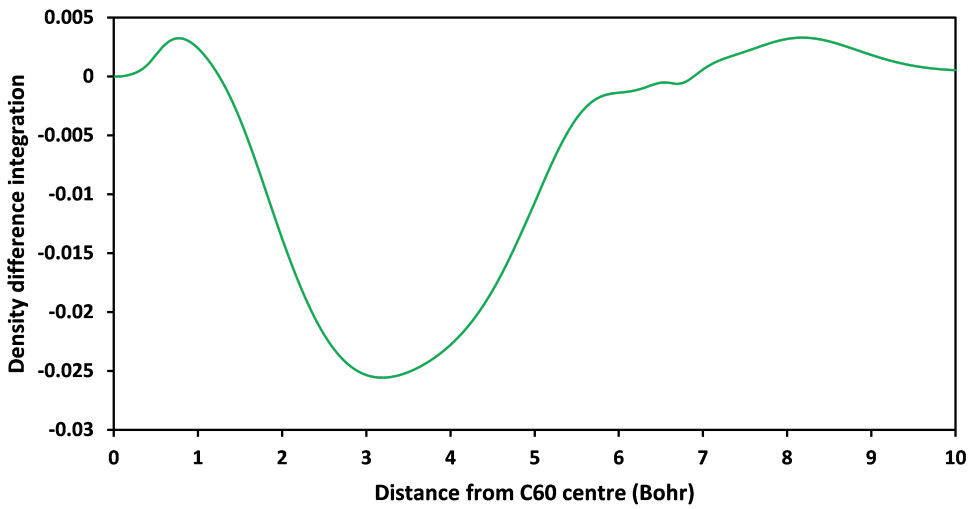

Figure 16: Radial difference of densities ($H_2O@C_{60}$-H_2O-C_{60}) from the C_{60} centre until the limit of the box

The difference in density is represented in figure 16, where the first region around 1.0 Bohr corresponds to the electron density reorganization in the water molecule. The section between 2 and 4, we find a minimal value around 3.2 Bohr, which is in agreement with the minimal point in

the density previously calculated. This value quantifies the charge transfer, because it gives the water density loss when it is placed in the C_{60} molecule. In this case, the charge transfer is around -0.025, and the negative value represent that the electron transfer is from the water to the C_{60}. Although we observe a charge transfer, the value is so small, that we can consider to be negligible.

5.3 Work in progress...

In this last chapter, I will talk about further studies we are working on. However, they cannot fully studied owing to the lack of time.

5.3.1 C60 filled with other molecules

After the study of the $H_2O@C_{60}$ system, other polar molecules have been studied by replacing water with hydrogen fluoride (HF), which is already synthesized [9], and also hydrogen iodide (HI). The strategy was the same as the water molecule, first of all we studied their behaviour in the centre of the fullerene.

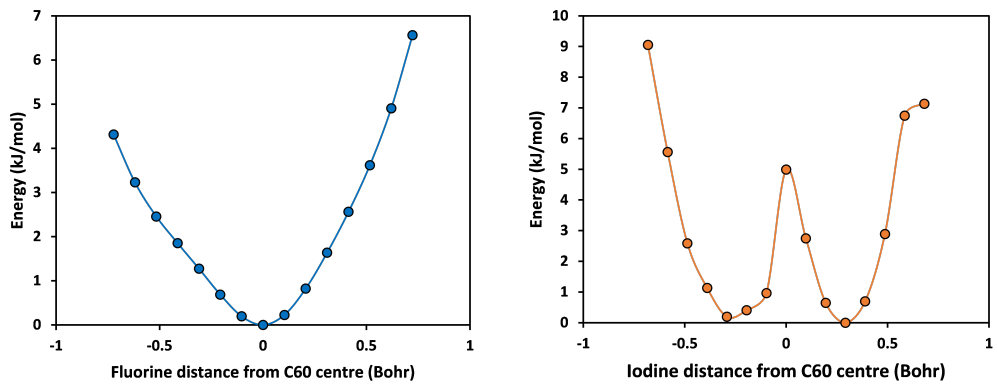

(a) Hydrogen fluorine **(b)** Hydrogen iodine

Figure 17: Energy diagram representation of fluoride of HF (left diagram), and iodide of HI (right diagram) in function of the distance from the C_{60} centre

Regarding the energy diagram of hydrogen fluoride represented in figure 17a, the most stable position for the fluorine is exactly in the centre of the C_{60} molecule, unlike of water's oxygen represented before in figure 10. Moreover, the right part of the plot, where the fluorine interacts with the C_{60}, the energy increases faster than the hydrogen interaction with the C_{60}. Therefore, the fluorine atom will be closer to the centre of the C_{60} molecule most of the time. This behaviour implies free rotation inside the C_{60}, interesting for the dipole moment fluctuation, which increases the dielectric constant.

On the other hand, the iodine is mildly shifted from the centre, see figure 17b. This plot shows some similarity to water's plot, but with a higher energy barrier. Moreover, the last point from the right side of the plot represents a reorientation of hydrogen iodine due to the proximity of the C_{60} surface, since its bond length ($HI \approx 3.01 \quad Bohr$) is larger than other two molecules, ($HF \approx 1.75 \quad Bohr, \quad and \quad H_2O \approx 1.82 \quad Bohr$), the hydrogen reach faster the C_{60} surface. Therefore, the free mobility region of hydrogen iodine will be small, obstructing the dipole fluctuation.

Concluding this section, the dipole moments of water, hydrogen fluoride, and hydrogen iodide systems were calculate, with resulting values of 0.52, 0.49, and 0.28 respectively. We observe that water and hydrogen fluoride have similar values, meanwhile, hydrogen iodine shows a lower dipole moment because of the relatively low electronegativity of iodine. Therefore, we can certainly conclude that the water and the hydrogen fluorine systems are more suitable to be included in organic photovoltaic as endofullerenes, rather than the hydrogen iodine.

5.3.2 Molecular dynamics

As we introduced at the beginning of this chapter, the dipolar contribution to the dielectric constant can be calculated by using molecular dynamics. The starting point was the forcefield by Monticelli [20] for C_{60} molecule, and the SPC model for water. Combining these two forcefields, the results did not show any relevant changes on the volume when a water molecule is introduced in the C_{60}, which are in agreement with the quantum mechanical calculation in crystal, and confirms the validity of this forcefield for the outer region (C_{60}-C_{60} interactions). However, the inner region (H_2O-C_{60}) is not validated for this reason was necessary a previous quantum mechanical study.

Therefore, the corresponding negative charge for C_{60} calculated with the DPA analysis must be included in the forcefield, and since water molecule can freely rotate in the C_{60}, the charge distribution of C_{60} should be able to change together with the water molecule. This generates a problem for standard forcefields, where the charges are fixed in the atoms, though this polarizability can be studied by using a polarizable forcefield.

Before focusing on the polarizable forcefield, several simulations were carried out with standard forcefield in order to analyse the sensitivity of the dielectric constant in function of molecules number:

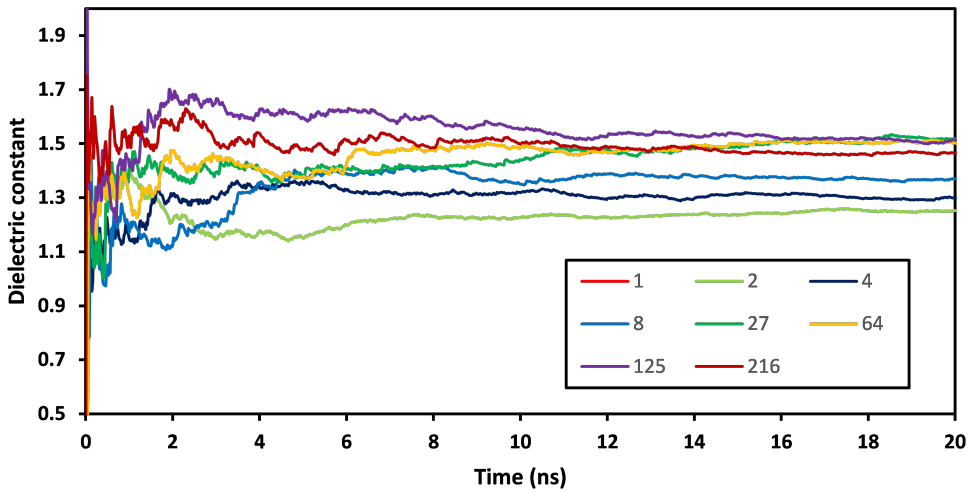

Figure 18: Dielectric constant evolution in function of the time, increasing the water@C60 molecules number from 1 to 216

As observed in figure 18, the dielectric constant converges to 1.5 in the simulation box with more than 27 molecules. Combining this results with the electronic contribution, the total dielectric constant would be 5.7, which is a quite high dielectric constant for organic photovoltaics cells, similar to PTEG-1. Moreover, calculations with a polarizable forcefield based on the Drude particle show a dipolar dielectric constant around 0.62, this value is lower than the calculated with the standard forcefield, but it is still high.

Coming back to the reality, quantum mechanical study showed that the dipole moment is considerably reduced when the water is confined within the C_{60}. Therefore, these forcefields completely neglects reduction of water polarity in the system. Therefore, this values cannot even be considered as real results until the forcefield (Lennard-Jones and Coulombic interactions) is validated, with the other quantum mechanical calculations.

6 Conclusions

This work focuses on the study of water molecule behaviour in the C_{60} by using quantum mechanical calculations. It demonstrates that the water have the sufficient space in the C_{60} to freely translate and rotate, which is highly desirable for dipoles fluctuations in order to increase the dielectric constant of the material.

Moreover, the DPA analysis has demonstrated a reduction of the dipole moment with respect to free water due to the polarization effect induced on the C_{60}.

The results from density calculations have proved the absence of charge transfer between C_{60} and water, concluding that the DPA charge obtained is related to the polarization.

Hydrogen fluoride and hydrogen iodide have been compared with water studies, where hydrogen fluorine has shown similar mobility and dipolar properties of water, which could be a suitable candidate for posterior studies. However, hydrogen iodine shows a reduced mobility and a relatively low dipole moment.

Concluding this project, the available forcefields cannot represent properly these kind of systems. Therefore, polarizable forcefields must be reparametrized in order to accurately describe the energies of water inside the C_{60}.

References

[1] Ellabban, O., Abu-Rub, H., & Blaabjerg, F. (2014). Renewable energy resources: Current status, future prospects and their enabling technology. Renewable and Sustainable Energy Reviews, 39, 748-764.

[2] PVeff(rev170117).png. (2017, March 23). Wikimedia Commons, the free media repository. Retrieved 12:37, June 15, 2017

[3] Palz, W. (1984). Kythnos Photovoltaic Power Plant. Photovoltaic Power Generation, 55-74.

[4] Frenkel, J. (1931). On the Transformation of Light into Heat in Solids. II. Physical Review, 37(10), 1276-1294.

[5] Exciton.png. (2017, February 19). Wikimedia Commons, the free media repository. Retrieved 12:40, June 15, 2017

[6] Gier, H. D., & Broer-Braam, H. B. (2016). Low exciton binding energies from computational predictions: towards the next generation of organic photovoltaics. Groningen: Rijksuniversiteit Groningen.

[7] Jahani, F., Torabi, S., Chiechi, R. C., Koster, L. J., & Hummelen, J. C. (2014). Fullerene derivatives with increased dielectric constants. Chemical Communications, 50(73), 10645.

[8] Sproul, A. B., Green, M. A., & Zhao, J. (1990). Improved value for the silicon intrinsic carrier concentration at 300 K. Applied Physics Letters, 57(3), 255-257.

[9] Krachmalnicoff, A., Bounds, R., Mamone, S., Alom, S., Concistr, M., Meier, B., . . . Whitby, R. J. (2016). The dipolar endofullerene HF@C60. Nature Chemistry, 8(10), 953-957.

[10] Kurotobi, K., & Murata, Y. (2011). A Single Molecule of Water Encapsulated in Fullerene C60. Science, 333(6042), 613-616.

[11] Carsten, B., Szarko, J. M., Son, H. J., Wang, W., Lu, L., He, F., . . . Yu, L. (2011). Examining the Effect of the Dipole Moment on Charge Separation in DonorAcceptor Polymers for Organic Photovoltaic Applications. Journal of the American Chemical Society, 133(50), 20468-20475.

[12] Kittel, C., & McEuen, P. (2015). Introduction to solid state physics. New Delhi: John Wiley & Sons.

[13] Huray, P. G. (2010). Maxwells Equations.

[14] Drude, P. (1902). Zur Elektronentheorie der Metalle. Annalen der Physik, 312(3), 687-692.

[15] Guest, M. F.; Bush, I. J.; Dam van, H. J. J.; Sherwood, P.; Thomas, J. M. H.; Lenthe van, J. H.; Havenith, R. W. A.; Kendrick, J. (2005). The GAMESS-UK Electronic Structure Package: Algorithms, Developments and Applications. Mol. Phys., 103, 719747.

[16] Grimme, S. (2006). Semiempirical GGA-type density functional constructed with a long-range dispersion correction. Journal of Computational Chemistry, 27(15), 1787-1799.

[17] Thole, B. T., & Duijnen, P. T. (1983). A general population analysis preserving the dipole moment. Theoretica Chimica Acta, 63(3), 209-221.

[18] Dovesi, R.; Orlando, R.; Erba, A.; Zicovich-Wilson, C. M.; Civalleri, B.; Casassa, S.; Maschio, L.; Ferrabone, M.; De La Pierre, M.; DArco, P.; Noel, Y.; Causa, M.; Rerat, M.; Kirtman, B. (2014). Int. J. Quantum Chem., 114, 1287-1317.

[19] Berendsen, H.J.C.; Spoel, D. & Drunen R., (1995). Gromacs - a Message-Passing Parallel Molecular-Dynamics Implementation. Computer Physics Communications, 91(1-3),43-56.

[20] Monticelli, L. (2012). On Atomistic and Coarse-Grained Models for C60Fullerene. Journal of Chemical Theory and Computation, 8(4), 1370-1378.

[21] Yannoni, C. S., Bernier, P. P., Bethune, D. S., Meijer, G., & Salem, J. R. (1991). NMR determination of the bond lengths in C60. Journal of the American Chemical Society, 113(8), 3190-3192.

[22] Jorgensen, W. L., Maxwell, D. S., & Tirado-Rives, J. (1996). Development and Testing of the OPLS All-Atom Force Field on Conformational Energetics and Properties of Organic Liquids. Journal of the American Chemical Society, 118(45), 11225-11236.

[23] Girifalco, L. A. (1992). Molecular properties of fullerene in the gas and solid phases. The Journal of Physical Chemistry, 96(2), 858-861.

[24] Berendsen, H. J., Grigera, J. R., & Straatsma, T. P. (1987). The missing term in effective pair potentials. The Journal of Physical Chemistry, 91(24), 6269-6271.

[25] Lamoureux, G., Harder, E., Vorobyov, I. V., Roux, B., & Mackerell, A. D. (2006). A polarizable model of water for molecular dynamics simulations of biomolecules. Chemical Physics Letters, 418(1-3), 245-249.

[26] G.Schaftenaar and J.H. Noordik,(2000). "Molden: a pre- and post-processing program for molecular and electronic structures", J. Comput.-Aided Mol. Design, 14, 123-134.

[27] Atkins, P. W. (2014). Atkins physical chemistry. Oxford: Oxford University Press.

[28] Mercer, P. R. (2016). More calculus of a single variable. Place of publication not identified: Springer-Verlag New York.